Available online at www.sciencedirect.com
ScienceDirect
Biochimica et Biophysica Acta 1768 (2007) 2300–2309
Biochimica et Biophysica Acta BBA
www.elsevier.com/locate/bbamem

Cholesterol modulation of membrane resistance to Triton X-100 explored by atomic force microscopy

Karim El Kirat [a], Sandrine Morandat [b,*]

[a] Laboratoire de Biomécanique et Génie Biomédical, UMR-CNRS 6600, Université de Technologie de Compiègne, BP 20529, 60205 Compiègne Cedex, France
[b] Laboratoire de Génie Enzymatique et Cellulaire, UMR-CNRS 6022, Université de Technologie de Compiègne, BP 20529, 60205 Compiègne Cedex, France

Received 29 January 2007; received in revised form 23 April 2007; accepted 3 May 2007
Available online 22 May 2007

Abstract

Biomembranes are not homogeneous, they present a lateral segregation of lipids and proteins which leads to the formation of detergent-resistant domains, also called "rafts". These rafts are particularly enriched in sphingolipids and cholesterol. Despite the huge body of literature on raft insolubility in non-ionic detergents, the mechanisms governing their resistance at the nanometer scale still remain poorly documented. Herein, we report a real-time atomic force microscopy (AFM) study of model lipid bilayers exposed to Triton X-100 (TX-100) at different concentrations. Different kinds of supported bilayers were prepared with dioleoylphosphatidylcholine (DOPC), sphingomyelin (SM) and cholesterol (Chol). The DOPC/SM 1:1 (mol/mol) membrane served as the non-resistant control, and DOPC/SM/Chol 2:1:1 (mol/mol/mol) corresponded to the raft-mimicking composition. For all the lipid compositions tested, AFM imaging revealed that TX-100 immediately solubilized the DOPC fluid phase leaving resistant patches of membrane. For the DOPC/SM bilayers, the remaining SM-enriched patches were slowly perforated leaving crumbled features reminiscent of the initial domains. For the raft model mixture, no holes appeared in the remaining SM/Chol patches and some erosion occurred. This work provides new, nanoscale information on the biomembranes' resistance to the TX-100-mediated solubilization, and especially about the influence of Chol.

Keywords: Raft; DRM; Real-time AFM; Lipid bilayer; Solubilization; Non-ionic detergent

1. Introduction

The plasma membrane of mammalian cells is mainly composed of glycerophospholipids (GPLs), sphingolipids (SphLs) and cholesterol (Chol) that are not homogeneously distributed within the bilayer as proposed by the fluid mosaic model [1] but they are rather organized into microdomains also called "rafts" [2,3]. These membrane microdomains are especially enriched in SphLs and Chol and they play a pivotal role in cellular processes such as signal transduction and membrane trafficking [4–8].

GPLs are especially enriched in unsaturated acyl chains that tend to adopt a kinked structure. Consequently, GPLs present a loosely packed conformation yielding a liquid-disordered or fluid phase (Ld or Lα) [9,10]. On the contrary to GPLs, SphLs bear long and saturated acyl chains. This property is responsible for their tight packing into gel phases in which only very little lateral diffusion can occur [11,12]. Furthermore, Chol can fill the voids between the acyl chains of SphLs leading to their association into a phase that is significantly more fluid than the gel phase: the liquid-ordered phase (Lo) [13–15].

Generally, rafts can be purified as detergent resistant membranes (DRMs) by cold extraction (4 °C) of eukaryotic cell plasma membranes. Usually, this protocol is based on the use of non-ionic detergents, such as Triton X-100 (TX-100) [3,5,16–18]. TX-100 has a low critical micelle concentration (CMC) of 0.24 mM and can also be useful for the purification and the reconstitution of integral or lipid modified proteins in biomembranes [19,20]. Furthermore, a growing body of literature describes model membranes mimicking DRMs such as liposomes, Langmuir monolayers or supported bilayers [21–26].

Atomic force microscopy (AFM) is a powerful technique that allows the high resolution imaging of biological specimens under physiologically compatible conditions (buffered solutions, temperature, …) [27]. Therefore, AFM is widely employed

* Corresponding author. Tel.: +33 3 44 23 44 18; fax: +33 3 44 20 39 10.
E-mail address: sandrine.morandat@utc.fr (S. Morandat).

0005-2736/$ - see front matter © 2007 Elsevier B.V. All rights reserved.
doi:10.1016/j.bbamem.2007.05.006

to explore phase separations in membranes [28] and the interaction of supported lipid bilayers with peptides [29–31], proteins [32–34], drugs [35], solvents [36] and buffers [37]. So far, only few articles have described detergent interaction with membranes observed by AFM [26,38–40]. In a previous study, TX-100 solubilization of dioleoylphosphatidylcholine/dipalmitoylphosphatidylcholine (DOPC/DPPC 1:1 mol/mol) bilayers was followed by AFM in real-time [39]. This lipid composition is known to produce fluid/gel phase separation at room temperature and can thus be considered as a simple model to investigate membrane resistance to detergents. Time-lapse AFM imaging revealed that when TX-100 was added at a concentration above the CMC, it was always able to dramatically alter DOPC/DPPC bilayers by instantly removing the DOPC fluid phase. The remaining DPPC gel phases then appeared more or less swollen depending on TX-100 concentration. The swelling of the gel domains was directly correlated with detergent intercalation within DPPC molecules. When DPPC gel phases were swollen, then holes appeared within the patches. This desorption of bilayer parts left the silhouette of the initial gel phase still recognizable even at the end of the incubation [39].

In this study, TX-100 solubilization of bilayers mimicking lipid rafts was followed in real-time by AFM. To this end, we have prepared three different bilayers: DOPC/sphingomyelin (SM) 1:1 (mol/mol), and DOPC/SM/Chol 2:1:1 (mol/mol/mol) or 4:3:1 (mol/mol/mol). Different TX-100 concentrations were tested to better understand its interaction with membranes.

2. Materials and methods

2.1. Materials

L-α-dioleoylphosphatidylcholine (DOPC), egg sphingomyelin (SM), cholesterol (Chol) and Triton X-100 were purchased from Sigma (St. Louis, MO) and used without any further purification. Other chemicals were purchased from Merck (Darmstadt, Germany). For all experiments, the distilled water was purified with a Millipore filtering system (Bedford, MA), yielding an ultrapure water with a resistivity of 18.2 MΩ × cm.

2.2. Preparation of supported lipid bilayers

Supported DOPC/SM 1:1 (mol/mol), DOPC/SM/Chol 4:3:1 (mol/mol/mol) and DOPC/SM/Chol 2:1:1 (mol/mol/mol) bilayers were prepared using the vesicle fusion method [26,41–43]. To this end, lipids were dissolved in chloroform at 1 mM final concentration. The mixture of these lipids was then evaporated under nitrogen and dried in a dessicator under vacuum for 2 h. Multilamellar vesicles (MLV) were obtained by resuspending the lipidic dried film at room temperature in a buffer containing calcium (10 mM Tris, 150 mM NaCl, 3 mM $CaCl_2$, pH 7.4; Tris/calcium buffer) at 1 mM final lipid concentration. To obtain small unilamellar vesicles (SUV), the suspension was sonicated to clarity (3 cycles of 2 min 30 s) using a 500 W titanium probe sonicator (Fisher Bioblock Scientific, France; 35% of the maximal power; 13 mm probe diameter) while being kept in an ice bath. The liposomal suspension was then filtered on a 0.2 μm Acrodisc® (Pall Life Sciences, USA) to eliminate titanium particles. Freshly cleaved mica squares (16 mm^2) were glued onto steel sample discs (Agar Scientific, England) using Epotek 377 (Polytec, France). A 150 μL portion of the SUV suspension was then deposited onto the mica samples, and the SUVs were allowed to adsorb and fuse on the solid surface for 1 h at 60 °C. Subsequently, samples were rinsed with 3 mL of buffer (10 mM Tris, 150 mM NaCl pH 7.4; Tris buffer) and slowly cooled to room temperature.

2.3. Atomic force microscopy

Supported bilayers were investigated using a commercial AFM (NanoScope III MultiMode AFM, Veeco Metrology LLC, Santa Barbara, CA) equipped with a 125 μm × 125 μm × 5 μm scanner (J-scanner). A quartz fluid cell was used without the O-ring. Topographic images were recorded in contact mode using oxide-sharpened microfabricated Si_3N_4 cantilevers (Microlevers, Veeco Metrology LLC, Santa Barbara, CA) with a spring constant of 0.01 N/m (manufacturer specified), with a minimal applied force (<200 pN) and at a scan rate of 5–6 Hz. The curvature radius of silicon nitride tips was ~20 nm. Images were obtained at room temperature (21–24 °C) either in a Tris buffer or in a Tris buffer containing TX-100. All images (256 × 256 pixel) shown in this paper are flattened raw data.

3. Results

DOPC/SM biomembranes were prepared with varying amounts of Chol. Preliminary experiments permitted to determine that DOPC/SM/Chol 1:1:1 (mol/mol/mol) produced interconnected small domains (data not shown) as previously described [26]. To allow the comparison among the different bilayers, we first managed to obtain well-delimited domains with a sufficient size (diameter between 2 and 15 μm). In the end, to better understand the mechanism of resistance to TX-100 related to the Chol content of membranes, we have selected three different lipid compositions. The DOPC/SM 1:1 (mol/mol) corresponded to the membrane easily solubilized by TX-100. The DOPC/SM/Chol 2:1:1 (mol/mol/mol) bilayer was considered as the raft-mimicking membrane. Indeed, as previously shown, the ternary mixture made of phospholipids with unsaturated acyl chains, sphingomyelin and cholesterol could crudely imitate the phase separation of cell membranes [12,15,21,32,34]. An intermediate composition was also tested: DOPC/SM/Chol 4:3:1 (mol/mol/mol). It is noteworthy that previous descriptions of these lipid compositions were shown to produce: gel phases of SM for the DOPC/SM membranes [26,44], and Lo phases of SM/Chol for the ternary mixtures [26,32]. These three lipid membranes were imaged by real-time AFM in buffer solution and in the presence of TX-100 at different concentrations.

3.1. Time-lapse AFM of DOPC/SM bilayers incubated with TX-100

Fig. 1A presents a typical AFM topographic image of a DOPC/SM bilayer. It reveals the coexistence of two phases: the brighter areas correspond to the domains enriched in SM forming a gel phase while the surrounding darker matrix can be attributed to DOPC in a fluid phase. SM domains protruded from the fluid phase by 1.0 ± 0.1 nm which is in accordance with previous descriptions of this lipid system [26,32,44].

Supported DOPC/SM bilayers were incubated with TX-100 at a concentration two times greater than the CMC (2CMC, 0.48 mM, Fig. 1A to D) and successive AFM images of the same area were then recorded: after 5, 30 and 120 min (Fig. 1B to D). Immediately after the TX-100 addition (Fig. 1B), the DOPC fluid phase was totally solubilized as attested by their thickness 5.5 ± 0.2 nm corresponding to apparently unmodified SM domains. At 30 min incubation time (Fig. 1C), the SM patches remained unaltered while some material, presumably

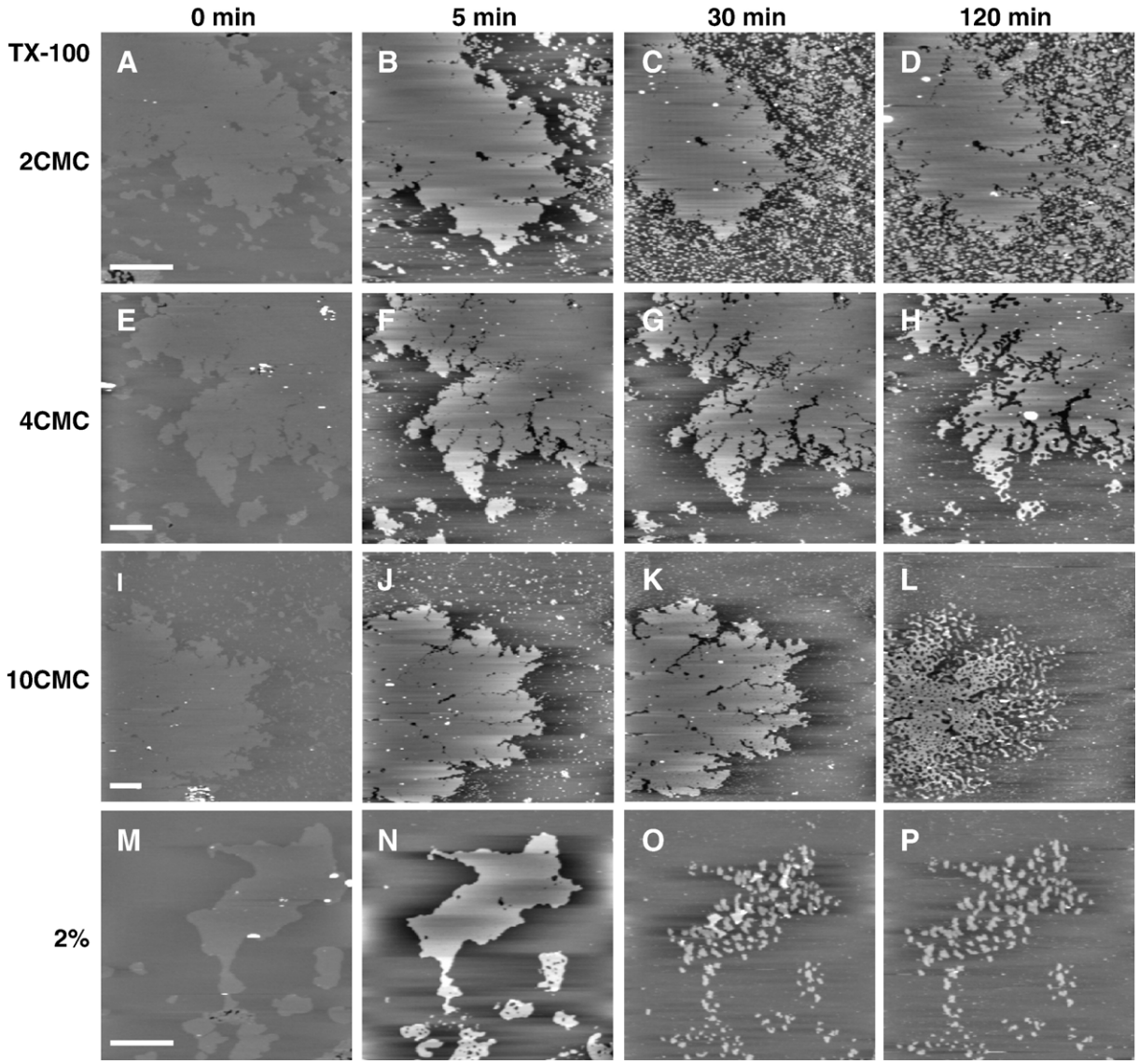

Fig. 1. TX-100 interaction with supported DOPC/SM 1:1 (mol/mol). AFM height images of mixed DOPC/SM 1:1 (mol/mol) bilayers were first recorded in Tris buffer before TX-100 addition (A, 10 μm × 10 μm; E, 15 μm × 15 μm; I, 20 μm × 20 μm and M, 10 μm × 10 μm). Different TX-100 concentrations were tested on each bilayer and images of the same area were acquired at different incubation times: 0.48 mM TX-100 (2CMC): (B) 5, (C), 30 and (D), 120 min; 0.96 mM TX-100 (4CMC): (F) 5, (G), 30 and (H), 120 min; 2.4 mM TX-100 (10CMC): (J) 5, (K), 30 and (L), 120 min; 2% TX-100 (v/v, 143CMC, 34 mM): (N) 5, (O), 30 and (P), 120 min. Scale bars are 2.5 μm and *z*-scale = 10 nm.

lipid/detergent complexes, began to readsorb onto the mica surface. After 120 min with 2CMC TX-100 (Fig. 1D), the shape of the SM domains was not modified, but meanwhile a lot of material redeposited on the mica. As this redeposition phenomenon was beyond the scope of this work, it was not further characterized.

Incubating DOPC/SM bilayers with TX-100 at a concentration four times greater than the CMC (4CMC, 0.96 mM, Fig. 1E to H) induced dramatic alterations of the bilayer. Indeed, just after detergent addition (Fig. 1F), the DOPC was completely removed leaving unchanged SM gel domains. As one can see in Fig. 1G (30 min), some holes appeared progressively at the edges of the remaining SM domains. After 120 min (Fig. 1H), the edge of SM patches was perforated but the overall size and shape of the domains remained identical.

DOPC/SM bilayers were also incubated with TX-100 at a concentration ten times greater than the CMC (10CMC, 2.4 mM, Fig. 1I to L). After 5 min (Fig. 1J), the DOPC fluid phase was completely removed leaving apparently unmodified SM patches. After 30 min (Fig. 1K), some holes were visible at the edge of the remaining SM patches. At 120 min incubation time (Fig. 1L), holes were spread on the overall SM domain and they were notably more distributed at the periphery. As a consequence, the distribution of the holes may result from a peripheral insertion of the detergent into the SM domain. However, it should be noticed that no swelling of the SM gel domains was observed just after detergent addition on the contrary to our previous work on DPPC gel patches [39]. To assess whether the detergent was able to enter the gel phase immediately as observed with DPPC swelling, the following

control experiment was done. TX-100 concentrated at 10CMC was added for 5 min to a DOPC/SM (1:1) bilayer and then extensively rinsed with Tris buffer to remove the detergent from the bulk. AFM real-time imaging revealed that no modifications of the SM gel domains were observed for 120 min (data not shown), thus indicating that hole formation observed in SM patches were due to a progressive insertion of the detergent at their edges. Moreover, as shown in Fig. 1L, after 120 min incubation, a new topographic level appeared with an intermediate height between the mica and the SM patch surface. The thickness of these newly produced patches was measured to be 3.7±0.2 nm and they seemed very stable because they kept the same size and thickness even after 120 min. In the same time, the height of the remaining SM domains was still conserved: 5.5±0.2 nm. It is also important to note that the silhouette of the initial SM gel domain was still recognizable even at the end of the incubation, indicating that the solubilization did not correspond to continuous erosion but rather to the sporadic removal of membrane patches.

A higher magnification of the images presented in Fig. 1I to L was obtained (Fig. 2) to gain a more detailed view on the evolution of the intermediate level. These AFM images were recorded between 30 and 120 min at 2.4 mM TX-100 (10CMC, Fig. 2A to E). From 30 min (Fig. 2A), very small holes were visible at the periphery of the SM patch. After 45 min (Fig. 2B), the perforations were larger with some of them presenting an elongated shape. After 60 min incubation time (Fig. 2C), very small holes were visible at the centre of the domain while stretched perforations were found at its edge. After 90 min (Fig. 2D), some thin patches began to appear at the periphery of the domain and corresponded to residual structures left by the desorption of the bilayer. Indeed, the boundary of the remaining SM gel domain presented elongated shapes prior to the formation of the intermediate level. At the final incubation time (120 min, Fig. 2E), most of the initial SM patch was desorbed leaving a lot of thin domains. The thin patches were always small, stable and localized at the periphery of the initial domain. These thin patches presented a step height of 3.7± 0.2 nm (Fig. 2F). According to this thickness, they might not be bilayers but rather monolayers of SM covered with monolayers of TX-100, or perhaps interdigitated SM molecules in the presence of high amounts of TX-100 [36]. These structures

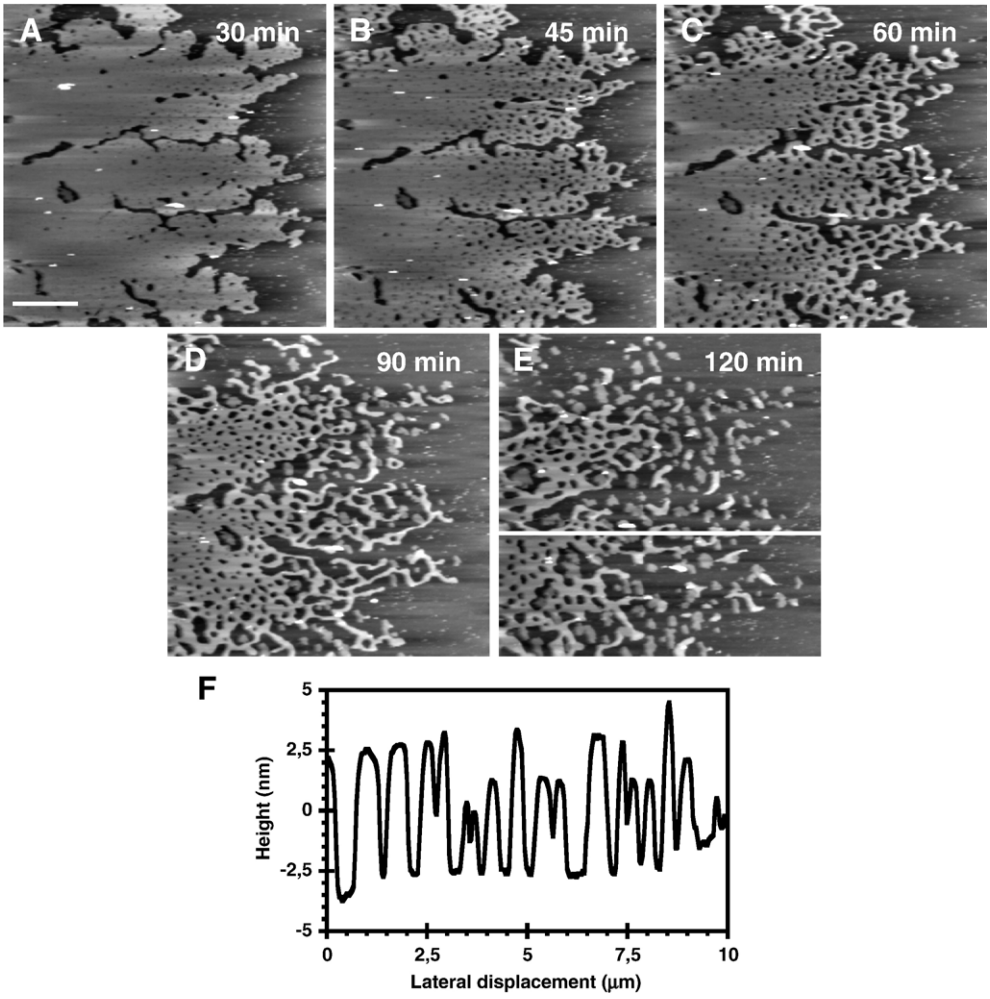

Fig. 2. Gel phase thinning induced by TX-100 interaction with supported DOPC/SM 1:1 (mol/mol). Higher magnification (10 µm × 10 µm) of the AFM height images presented in Fig. 1I to L. The same area was imaged at different incubation times: (A) 30, (B) 45, (C) 60, (D) 90 and (E) 120 min. The cross section analysis (F) corresponds to the white line in the panel (E). Scale bar is 2.5 µm and *z*-scale = 10 nm.

might be artifactual since the supported membrane is in interaction with the mica surface. Even if there is a thin water compartment (~1–2 nm) between the bilayer and the mica [42,45–47], the diffusion of the lipids in the membrane lower leaflet might be limited [48]. The formation of this thin patch may be due to different diffusion velocities of TX-100 between the upper and the lower leaflet of SM patches. So, TX-100 molecules may accumulate faster in the upper leaflet while they diffuse slower in the lower leaflet due to a closer contact with the mica substrate. It may then provoke the desorption of mixed micelles essentially from the upper part of the membrane, leaving the lower part stabilized by the interaction with TX-100 molecules having a large polar head. Even if there is an obvious influence of the mica substrate, one may also notice that such thinning was never observed with other compositions than DOPC/SM. This suggests that the membrane thinning is directly related to specific properties of SM in gel phase.

A supported bilayer of DOPC/SM 1:1 (mol/mol) was incubated in the presence of TX-100 at a concentration of 2% (v/v) (i.e. 143CMC, 34 mM, Fig. 1M to P) corresponding to the classical concentration chosen to purify biological membrane fractions resistant to detergent solubilization at 4 °C [18,49]. As one can see in Fig. 1N, within the first 5 min, holes began to appear in the smallest remaining SM domains. After 30 min (Fig. 1O), the domains were completely crumbled and the level corresponding to SM almost totally disappeared leaving new time-stable thin patches with 3.7±0.2 nm height. These thin domains were stable in time as observed after 120 min (Fig. 1P).

It is important to note that supported DOPC/SM 1:1 (mol/mol) bilayers incubated with TX-100 below the CMC, at 0.12 mM (CMC/2) showed no effect of the detergent (data not shown). Indeed, both fluid and gel phases remained apparently unaltered for 120 min.

3.2. Time-lapse AFM of DOPC/SM/Chol (2:1:1) bilayers incubated with TX-100

To form a Lo phase, cholesterol was added to the DOPC/SM mixture. The ternary mixtures of DOPC/SM/Chol have been previously used as a model in the study of lipid rafts [21,26,32]. AFM images of DOPC/SM/Chol 2:1:1 (mol/mol/mol) supported bilayers permitted to observe a phase separation (Fig. 3A, E and I) with well-delimited domains and no interconnections. The height difference between the phases was 0.8±0.1 nm which is consistent with previous descriptions of this ternary lipid system [26].

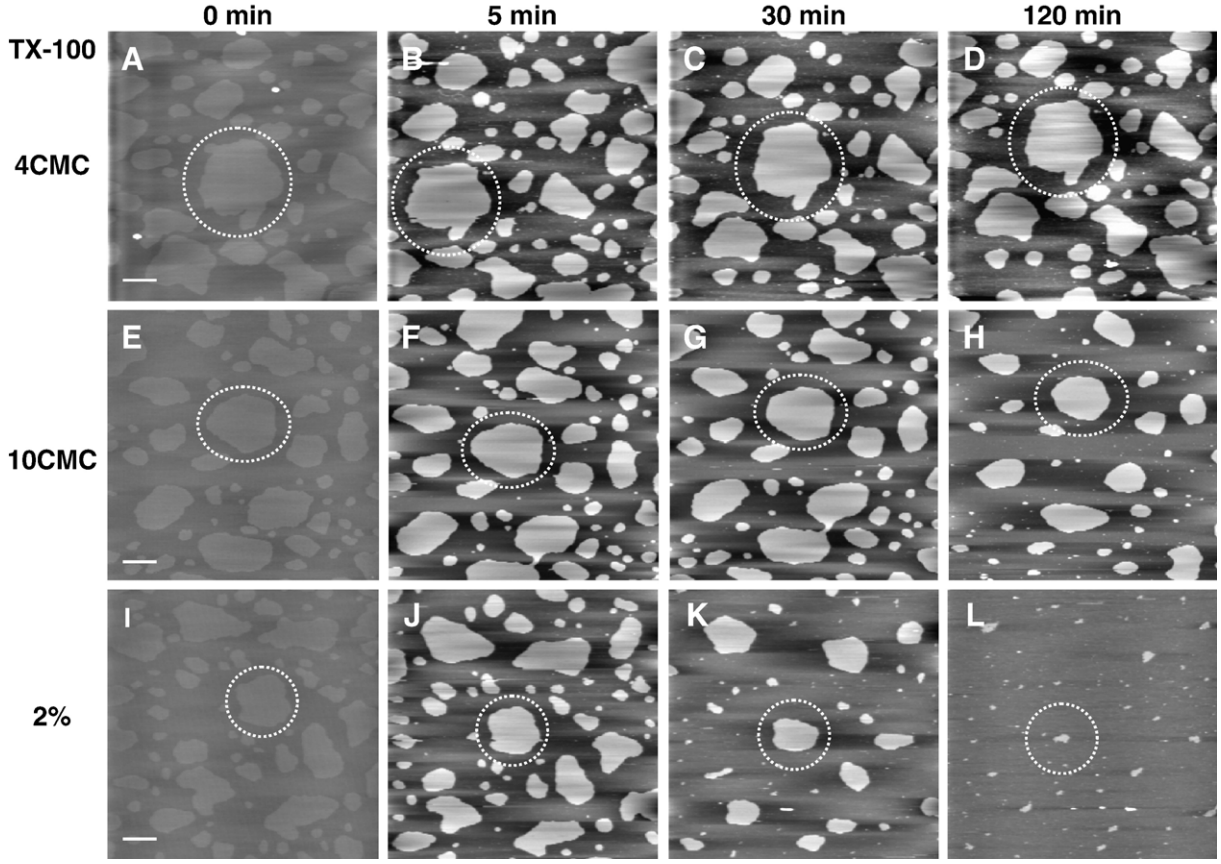

Fig. 3. TX-100 interaction with supported DOPC/SM/Chol 2:1:1 (mol/mol/mol). AFM height images (20 μm × 20 μm) of mixed DOPC/SM/Chol 2:1:1 (mol/mol/mol) bilayers were first recorded in Tris buffer before TX-100 addition (A, E and I). Different TX-100 concentrations were tested on each bilayer and images of the same area were acquired at different incubation times: 0.96 mM TX-100 (4CMC): (B) 5, (C), 30 and (D), 120 min; 2.4 mM TX-100 (10CMC): (F) 5, (G), 30 and (H), 120 min; 2% TX-100 (v/v, 143CMC, 34 mM): (J) 5, (K), 30 and (L), 120 min. Scale bars are 2.5 μm and *z*-scale = 10 nm.

To study the resistance of rafts mimics to detergent solubilization, DOPC/SM/Chol 2:1:1 (mol/mol/mol) bilayers were incubated with TX-100 at different concentrations. These membranes were first incubated with TX-100 at a concentration corresponding to 4CMC (Fig. 3A to D). At 5 min (Fig. 3B), the DOPC fluid phase was immediately removed upon TX-100 addition whereas the Lo domains remained unaltered. After 30 min (Fig. 3C), no modifications of the remaining Lo patches were visible. At longer incubation time (120 min, Fig. 3D), no erosion or holes were observed, the Lo patches seemed to resist the solubilization by TX-100 at a concentration corresponding to 4CMC.

Fig. 3E to H corresponds to raft-mimicking bilayers incubated with TX-100 at a concentration of 10CMC. As one can see in Fig. 3F, 5 min after TX-100 addition, the DOPC fluid phase was completely removed leaving unmodified SM/Chol Lo patches. At 30 min incubation time (Fig. 3G), the Lo patches were still unaffected as no erosion and no holes could be observed. However, after 120 min (Fig. 3H), the domains were considerably eroded at their border by the detergent action. No holes appeared within the domains indicating that the detergent could not enter the Lo phase except at their edges in a moderate way.

This solubilization by centripetal erosion of the Lo domains was confirmed by using a solution of 2 vol.% TX-100 (143CMC, 34 mM; Fig. 3I to L). Immediately after the addition of detergent (5 min, Fig. 3J), the DOPC fluid phase was completely desorbed and even at 2 vol.% TX-100, no modification of the remaining Lo SM/Chol patches could be observed. After 30 min (Fig. 3K), a massive erosion occurred but it is noteworthy that even at very high detergent concentration, no holes appeared within the Lo phases. At 120 min (Fig. 3L), the erosion phenomenon ended as there were no more Lo patches left on the mica surface.

To confirm that the erosion of the Lo domains took place by successive insertion of TX-100 at their periphery, a control experiment was done by adding the detergent at a concentration of 10CMC for 5 min to a DOPC/SM/Chol 2:1:1 (mol/mol/mol) bilayer. The sample was then extensively rinsed with a Tris buffer to remove the detergent from the bulk. No modifications of the gel domains were observed after 120 min (data not shown) indicating that the erosion phenomenon described above was not due to TX-100 molecules pre-inserted into the Lo phase.

Supported DOPC/SM/Chol 2:1:1 (mol/mol/mol) bilayers were also incubated with TX-100 at 0.12 mM (CMC/2). Under these conditions, i.e. below the CMC of TX-100, the DOPC fluid phase and the SM/Chol Lo domains appeared unaltered for 120 min (data not shown).

3.3. Time-lapse AFM of DOPC/SM/Chol (4:3:1) bilayers incubated with TX-100

To test the influence of Chol content on the resistance of membranes to TX-100 solubilization, the ternary mixture DOPC/SM/Chol 4:3:1 (mol/mol/mol) was prepared. As previously observed with the DOPC/SM/Chol 2:1:1 (mol/mol/mol) mixture, the DOPC/SM/Chol 4:3:1 (mol/mol/mol) bilayer exhibited a phase separation with brighter domains corresponding to the Lo phase enriched in SM and Chol (step height of 0.9±0.1 nm) (Fig. 4).

This intermediate DOPC/SM/Chol composition was incubated with TX-100 at a concentration of 4CMC (Fig. 4A to D). Just after detergent addition (5 min, Fig. 4B), the DOPC fluid phase was solubilized while the SM/Chol Lo domains remained unmodified. After 30 min (Fig. 4C), a slow erosion phenomenon took place at the edges of the Lo domains. At 120 min incubation time (Fig. 4D), the erosion process was still far from completion and no holes were visible on the domains.

These membranes were also incubated with TX-100 at a concentration of 10CMC (Fig. 4E to H). After 5 min (Fig. 4F), the fluid phase was completely desorbed while the Lo domains were immediately perforated. The Lo domains were simultaneously perforated and eroded leaving smaller patches on the mica surface after 30 min (Fig. 4G). At 120 min incubation time (Fig. 4H), the remaining Lo patches were completely unrecognizable with their smooth edges.

DOPC/SM/Chol 4:3:1 (mol/mol/mol) bilayers were incubated with a 2% (v/v) TX-100 solution (143CMC, 34 mM, Fig. 4I to L). Again, after 5 min (Fig. 4J), the DOPC phase was completely removed while the Lo patches were perforated. After 30 min (Fig. 4K), the Lo perforated domains were strongly modified by centripetal erosion and they were no longer recognizable. At 120 min (Fig. 4L), no Lo domains were found left on the mica surface, the erosion was then completed. It is important to note that, on the contrary to the DOPC/SM 1:1 molar ratio, no thin patches were found on the surface after the solubilization of the bilayers composed of DOPC/SM/Chol 4:3:1 (mol/mol/mol).

These results corroborate that this Chol concentration present a solubilization behavior that is intermediate between the DOPC/SM 1:1 (mol/mol) and the DOPC/SM/Chol 2:1:1 (mol/mol/mol) bilayers. Indeed, with the 4:3:1 composition, we have observed at the same time: some perforations, which are characteristic of the DOPC/SM 1:1 molar ratio, and the erosion of the Lo patches, which corresponds to the behavior of the detergent resistant mixture DOPC/SM/Chol 2:1:1 (mol/mol/mol).

4. Discussion

Understanding the factors governing biomembranes' solubilization at the molecular level is essential in biophysics, biochemistry and cell biology. Especially in the case of rafts, examining the molecular determinants responsible for their insensitivity to TX-100 solubilization might clarify the mechanisms of membrane solubilization. In these experiments, we have tested the resistance to TX-100 of model membranes with different lipid molar ratios: DOPC/SM 1:1, DOPC/SM/Chol 4:3:1 and the 2:1:1 raft-mimicking composition. These AFM real-time imaging experiments permitted to observe the mechanism of biomembranes' solubilization at the nanoscale and also to confirm the pivotal influence of the Chol content.

At a concentration above the CMC, whatever the lipid composition, the first step of TX-100 solubilization always consisted in the complete removal of the DOPC fluid phase (Fig.

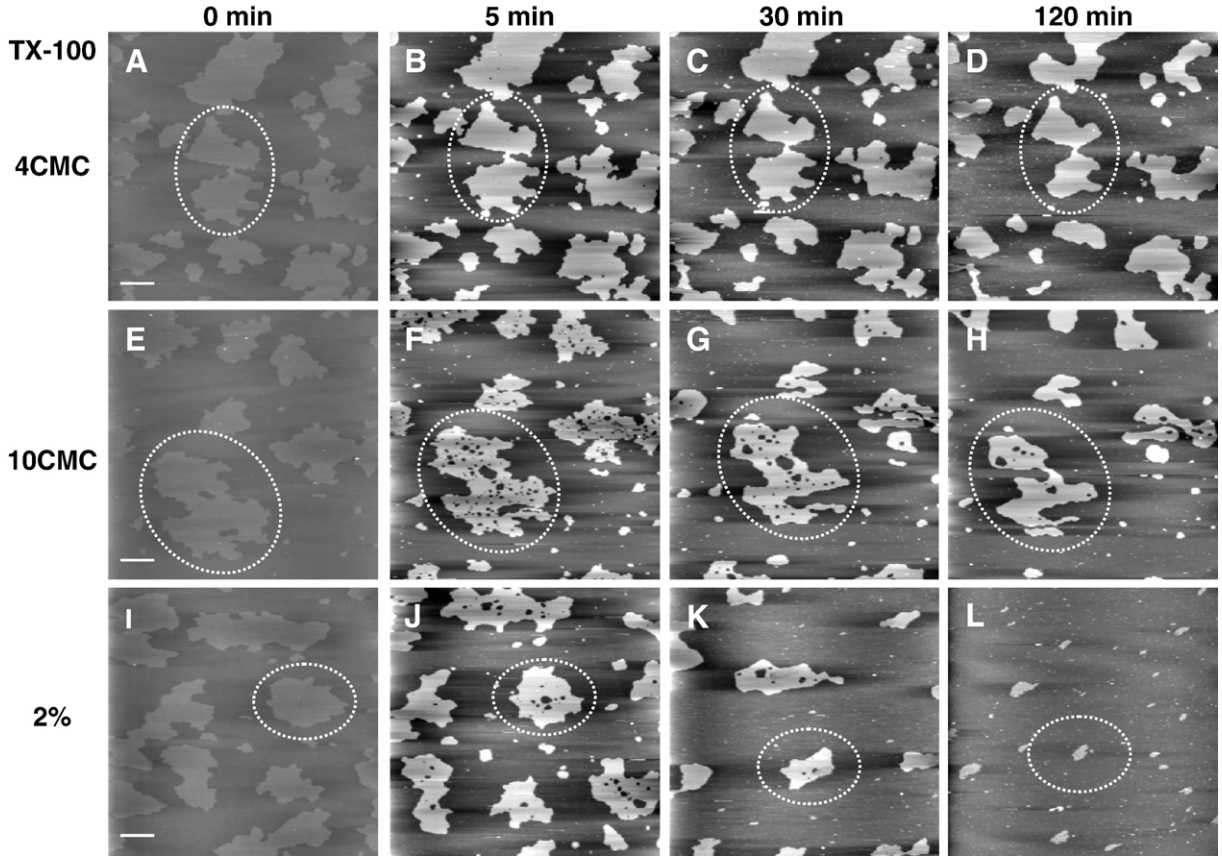

Fig. 4. TX-100 interaction with supported DOPC/SM/Chol 4:3:1 (mol/mol/mol). AFM height images (20 μm × 20 μm) of mixed DOPC/SM/Chol 4:3:1 (mol/mol/mol) bilayers were first recorded in Tris buffer before TX-100 addition (A, E, and I). Different TX-100 concentrations were tested on each bilayer and images of the same area were acquired at different incubation times: 0.96 mM TX-100 (4CMC): (B) 5, (C), 30 and (D), 120 min; 2.4 mM TX-100 (10CMC): (F) 5, (G), 30 and (H), 120 min; 2% TX-100 (v/v, 143CMC, 34 mM): (J) 5, (K), 30 and (L), 120 min. Scale bars are 2.5 μm and *z*-scale = 10 nm.

5A and B). Indeed, this early event always left membrane patches easily recognizable as the SM gel domains for the DOPC/SM composition, or as the SM/Chol Lo phases for the ternary DOPC/SM/Chol mixtures (see Fig. 5A ii and B ii). The comparison of the results obtained for the DOPC/SM system and the raft-mimicking membranes is clear evidence of two markedly different solubilization pathways. For the non-resistant membrane of DOPC/SM, the solubilization occurred by the sporadic removal of bilayer patches from the remaining SM gel domains (Fig. 5A ii to 5A iii). This mechanism left crumbled domains with their silhouette reminiscent of the initial SM gel phase even at the end of the solubilization. It is also important to note that no swelling of the SM gel domains occurred, at any TX-100 concentration, on the contrary to the previously described DPPC gel patches [39]. This difference with DPPC may arise from the abundant H bonds formed among SM polar heads as previously shown [50–53]. These bonds between the NH and OH groups of SM molecules might strengthen the gel phase by providing a better chain stacking thus avoiding the swelling attributable to TX-100 massive infiltration. As the SM gel phase was not able to incorporate high amounts of TX-100 molecules, it was not solubilized as fast as DPPC swollen gel patches [39]. However, the gel domains of DPPC and SM were desorbed in the same fashion by the formation of holes proportionately to TX-100 concentration. Another similarity between DPPC and SM gel phases is the observation of some residual patches leaving a silhouette reminiscent of the initial domain.

When the rafts mimicking membranes DOPC/SM/Chol 2:1:1 (mol/mol/mol) were incubated with TX-100, no holes could be observed in the Lo SM/Chol patches (Fig. 5B). On the contrary to the SM gel domains, the solubilization of the SM/Chol Lo patches took place only at their boundaries and without any perforation (Fig. 5B ii and iii). This main difference may be attributed to the ability of Chol to fill the voids between the sphingolipids' acyl chains thus inducing an increased packing density of SM molecules [13,51]. As Chol was able to fill the voids, then TX-100 had no way to enter the Lo phase. Consequently, Lo patches were eroded only by progressive destabilization at their edges where the lipid packing was disturbed. Indeed, even for TX-100 at a concentration of 2% (v/v; i.e. 143CMC, 34 mM), which is the classical concentration required for the preparation of DRMs from biological membranes, the Lo patches were only eroded by their side as no holes were visible (Fig. 5B iii).

Therefore, there are two different TX-100-mediated solubilization pathways: (i) for non-resistant membranes, solubilization occurs by hole formation and the crumbling of the gel domains (Fig. 5A); and (ii) for resistant membranes, TX-100 erodes the bilayer patches visibly without affecting their center (Fig. 5B).

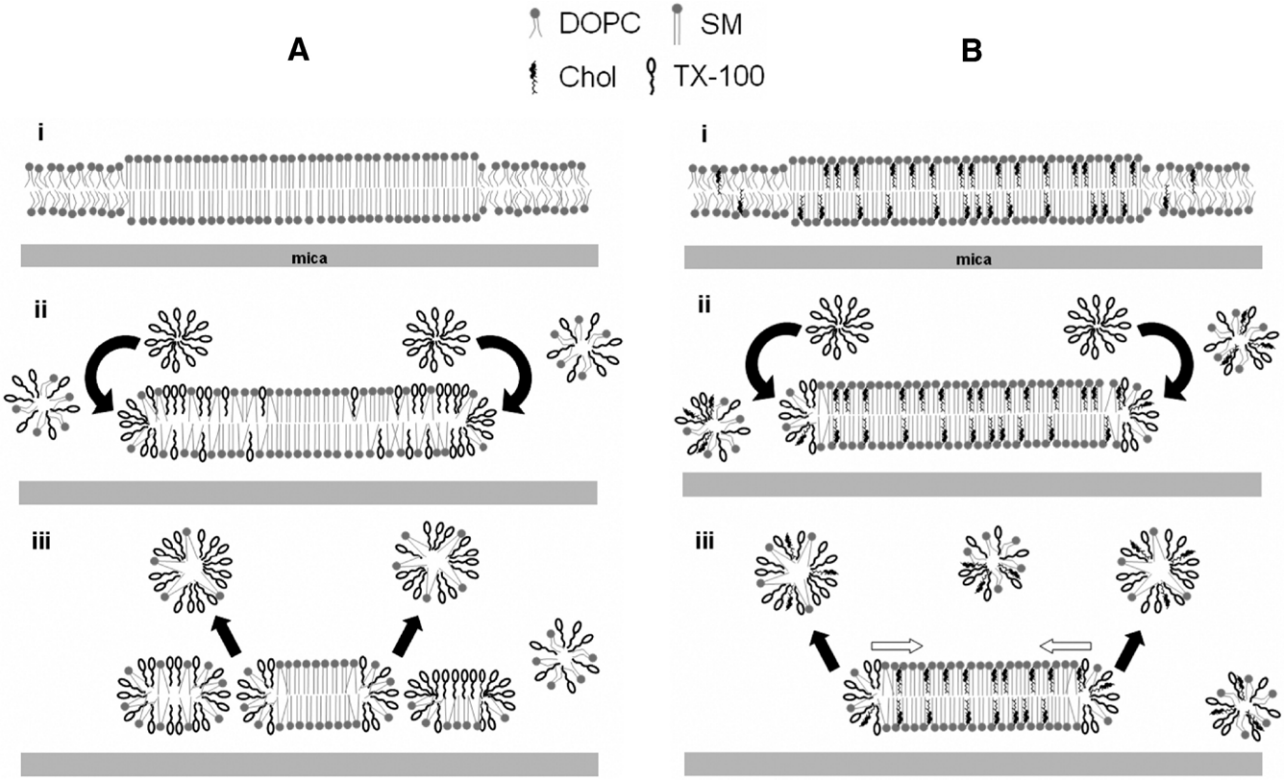

Fig. 5. Schematic mechanism proposed to describe the interaction of TX-100 with biomembranes. On the basis of our AFM experiments, we can distinguish two kinds of biomembranes according to their resistance to the solubilization by TX-100, and to the mode of desorption of the bilayer at the nanometer scale. The first situation (panel A) is encountered when the membrane is not resistant to TX-100. Typically, the DOPC/SM 1:1 molar mixture is not resistant to TX-100 and it forms a phase separation with a gel phase enriched in SM and a surrounding fluid phase essentially composed of DOPC (A i). When TX-100 is added at a concentration above its CMC to the bilayer, it induces the immediate desorption of DOPC leaving apparently unmodified SM gel patches (A ii). Then the micelles of TX-100 are able to insert at the boundaries of the remaining SM patches, and TX-100 molecules may diffuse within the domain (A ii). As they may be more concentrated on the edges than at the center, one can observe the formation of holes with a centripetal distribution. It may result in the sporadic desorption of small patches of SM/TX-100, leaving a crumbled domain with a silhouette reminiscent of the initial SM domain (A iii). The second situation (panel B) corresponds to a biomembrane resistant to TX-100, for example with the DOPC/SM/Chol 2:1:1 (mol/mol/mol). This bilayer present a phase separation with an ordered fluid phase Lo mainly composed of SM/Chol surrounded by DOPC in the fluid phase (B i). It is noteworthy that Chol intercalation between SM molecules permit to fill the voids (B i). Immediately after TX-100 addition to the membrane, the DOPC fluid phase is completely removed leaving an apparently unaffected SM/Chol Lo phase (B ii). At this step, the micelles enriched in TX-100 may be able to enter the remaining patch only at its edge. Due to the presence of intercalated Chol, TX-100 molecules are not able to diffuse within the domain, so that they become enriched at the edges and they provoke the centripetal erosion of the bilayer patch (B iii).

As a further proof of the existence of these two solubilization pathways, the intermediate composition DOPC/SM/Chol 4:3:1 (mol/mol/mol) was tested. For this lipid mixture, we have obtained both the holes and the erosion mechanisms. The dual solubilization behavior of these bilayers confirmed that they were intermediate between the TX-100 sensitive (DOPC/SM) and the TX-100 resistant (raft-mimicking) lipid mixtures. This intermediate mixture confirms the requirement for a minimum amount of Chol mixed with SM to provide a good resistance to TX-100 solubilization, when all the voids between SM molecules are properly filled with Chol.

5. Conclusion

In this study, we have reported the monitoring of membrane solubilization by the non-ionic detergent TX-100, in real-time at the nanometer scale. Again, AFM showed its effectiveness in providing original insights into biologically relevant events at the molecular level. Besides the confirmation of previous macro- and microscale observations, we believe that these AFM experiments will permit one to gain a better understanding of the determinants influencing raft membrane resistance to non-ionic detergents at the nanometer level.

Acknowledgements

The support of the Centre National de la Recherche Scientifique (CNRS), of the french research ministry, and of the Université de Technologie de Compiègne (UTC, Plan de Pluriformation « PPF Nanobiotechnologies ») is gratefully acknowledged. The authors thank the Service d'Analyses Physico-Chimiques of UTC for the use of the atomic force microscope.

References

[1] S.J. Singer, G.L. Nicolson, The fluid mosaic model of the structure of cell membranes, Science 175 (1972) 720–731.

[2] K. Simons, G. van Meer, Lipid sorting in epithelial cells, Biochemistry 27 (1988) 6197–6202.
[3] K. Simons, E. Ikonen, Functional rafts in cell membranes, Nature 387 (1997) 569–572.
[4] K. Simons, D. Toomre, Lipid rafts and signal transduction, Nat. Rev., Mol. Cell Biol. 1 (2000) 31–39.
[5] D.A. Brown, E. London, Structure and function of sphingolipid- and cholesterol-rich membrane rafts, J. Biol. Chem. 275 (2000) 17221–17224.
[6] W.I. Lencer, D. Saslowsky, Raft trafficking of AB5 subunit bacterial toxins, Biochim. Biophys. Acta 1746 (2005) 314–321.
[7] D.R. Taylor, N.M. Hooper, The prion protein and lipid rafts, Mol. Membr. Biol. 23 (2006) 89–99.
[8] T. Cinek, V. Horejsi, The nature of large noncovalent complexes containing glycosyl-phosphatidylinositol-anchored membrane glycoproteins and protein tyrosine kinases, J. Immunol. 149 (1992) 2262–2270.
[9] G. Radeva, F.J. Sharom, Isolation and characterization of lipid rafts with different properties from RBL-2H3 (rat basophilic leukaemia) cells, Biochem. J. 380 (2004) 219–230.
[10] E. London, D.A. Brown, Insolubility of lipids in triton X-100: physical origin and relationship to sphingolipid/cholesterol membrane domains (rafts), Biochim. Biophys. Acta 1508 (2000) 182–195.
[11] P. Niemela, M.T. Hyvonen, I. Vattulainen, Structure and dynamics of sphingomyelin bilayer: insight gained through systematic comparison to phosphatidylcholine, Biophys. J. 87 (2004) 2976–2989.
[12] E. London, How principles of domain formation in model membranes may explain ambiguities concerning lipid raft formation in cells, Biochim. Biophys. Acta 1746 (2005) 203–220.
[13] T. Harder, K. Simons, Caveolae, DIGs, and the dynamics of sphingolipid–cholesterol microdomains, Curr. Opin. Cell Biol. 9 (1997) 534–542.
[14] S. Munro, Lipid rafts: elusive or illusive? Cell 115 (2003) 377–388.
[15] T.P. McMullen, R.N. Lewis, R.N. McElhaney, Cholesterol–phospholipid interactions, the liquid-ordered phase and lipid rafts in model and biological membranes, Curr. Opin. Colloid Interface Sci. 8 (2004) 459–468.
[16] L.J. Pike, X. Han, K.N. Chung, R.W. Gross, Lipid rafts are enriched in arachidonic acid and plasmenylethanolamine and their composition is independent of caveolin-1 expression: a quantitative electrospray ionization/mass spectrometric analysis, Biochemistry 41 (2002) 2075–2088.
[17] R.J. Schroeder, E. London, D.A. Brown, Insaturations between saturated acyl chains confer detergent resistance on lipids and glycosylphosphatidylinositol (GPI)-anchored proteins: GPI-anchored proteins in liposomes and cells show similar behaviour, Proc. Natl. Acad. Sci. U. S. A. 91 (1994) 12130–12134.
[18] S. Bonnin, K. El Kirat, M. Becchi, M. Dubois, C. Grangeasse, C. Giraud, A.F. Prigent, M. Lagarde, B. Roux, F. Besson, Protein and lipid analysis of detergent-resistant membranes isolated from bovine kidney, Biochimie 85 (2003) 1237–1244.
[19] S. Morandat, M. Bortolato, B. Roux, Cholesterol-dependent insertion of glycosylphosphatidylinositol-anchored enzyme, Biochim. Biophys. Acta 1564 (2002) 473–478.
[20] J.L. Rigaud, M.T. Paternostre, A. Bluzat, Mechanisms of membrane protein insertion into liposomes during reconstitution procedures involving the use of detergents. 2. Incorporation of the light-driven proton pump bacteriorhodopsin, Biochemistry 27 (1988) 2677–2688.
[21] C. Dietrich, L.A. Bagatolli, Z.N. Volovyk, N.L. Thompson, M. Levi, K. Jacobson, E. Gratton, Lipid rafts reconstituted in model membranes, Biophys. J. 80 (2001) 1417–1428.
[22] S.N. Ahmed, D.A. Brown, E. London, On the origin of sphingolipid/cholesterol-rich detergent-insoluble cell membranes: physiological concentrations of cholesterol and sphingolipid induce formation of a detergent-insoluble, liquid-ordered lipid phase in model membranes, Biochemistry 36 (1997) 10944–10953.
[23] S. Morandat, M. Bortolato, B. Roux, Role of GPI-anchored enzyme in liposome detergent-resistance, J. Membr. Biol. 191 (2003) 215–221.
[24] R.J. Schroeder, S.N. Ahmed, Y. Zhu, E. London, D.A. Brown, Cholesterol and sphingolipid enhance the Triton X-100 insolubility of glycosylphosphatidylinositol-anchored proteins by promoting the formation of detergent-insoluble ordered membrane domains, J. Biol. Chem. 273 (1998) 1150–1157.
[25] T. Nyholm, J.P. Slotte, Comparison of Triton X-100 penetration into phosphatidylcholine and sphingomyelin mono- and bilayers, Langmuir 17 (2001) 4724–4730.
[26] H.A. Rinia, M.M. Snel, J.P. van der Eerden, B. de Kruijff, Visualizing detergent resistant domains in model membranes with atomic force microscopy, FEBS Lett. 501 (2001) 92–96.
[27] D.J. Muller, H. Janovjak, T. Lehto, L. Kuerschner, K. Anderson, Observing structure, function and assembly of single proteins by AFM, Prog. Biophys. Mol. Biol. 79 (2002) 1–43.
[28] Y.F. Dufrene, W.R. Barger, J.-B.D. Green, G.U Lee, Nanometer-scale surface properties of mixed phospholipid monolayers and bilayers, Langmuir 13 (1997) 4779–4784.
[29] K. El Kirat, L. Lins, R. Brasseur, Y.F. Dufrene, Fusogenic tilted peptides induce nanoscale holes in supported phosphatidylcholine bilayers, Langmuir 21 (2005) 3116–3121.
[30] K. El Kirat, L. Lins, R. Brasseur, Y.F. Dufrene, Nanoscale modification of supported lipid:membranes: synergistic effect of phospholipase D and viral fusion peptide, J. Biomed. Nanotech. 1 (2005) 39–46.
[31] K. El Kirat, Y.F. Dufrene, L. Lins, R. Brasseur, The SIV tilted peptide induces cylindrical reverse micelles in supported lipid bilayers, Biochemistry 45 (2006) 9336–9341.
[32] P.E. Milhiet, M.C. Giocondi, O. Baghdadi, F. Ronzon, B. Roux, C. Le Grimellec, Spontaneous insertion and partitioning of alkaline phosphatase into model lipid rafts, EMBO Rep. 3 (2002) 485–490.
[33] N.A. Geisse, B. Wasle, D.E. Saslowsky, R.M. Henderson, J.M. Edwardson, Syncollin homo-oligomers associate with lipid bilayers in the form of doughnut-shaped structures, J. Membr. Biol. 189 (2002) 83–92.
[34] D.E. Saslowsky, J. Lawrence, X. Ren, D.A. Brown, R.M. Henderson, J.M. Edwardson, Placental alkaline phosphatase is efficiently targeted to rafts in supported lipid bilayers, J. Biol. Chem. 277 (2002) 26966–26970.
[35] G. Mao, D. Chen, H. Handa, W. Dong, D.G. Kurth, H. Mohwald, Deposition and aggregation of aspirin molecules on a phospholipid bilayer pattern, Langmuir 21 (2005) 578–585.
[36] J. Mou, J. Yang, C. Huang, Z. Shao, Alcohol induces interdigitated domains in unilamellar phosphatidylcholine bilayers, Biochemistry 33 (1994) 9981–9985.
[37] J. Mou, J. Yang, Z. Shao, Tris(hydroxymethyl)aminomethane (C4H11NO3) induced a ripple phase in supported unilamellar phospholipid bilayers, Biochemistry 33 (1994) 4439–4443.
[38] S. Morandat, K. El Kirat, Solubilization of supported lipid membranes by octyl glucoside observed by time-lapse atomic force microscopy, Colloids Surf., B 55 (2007) 179–184.
[39] S. Morandat, K. El Kirat, Membrane resistance to Triton X-100 explored by real-time atomic force microscopy, Langmuir 22 (2006) 5786–5791.
[40] P.E. Milhiet, F. Gubellini, A. Berquand, P. Dosset, J.L. Rigaud, C. Le Grimellec, D. Levy, High-resolution AFM of membrane proteins directly incorporated at high density in planar lipid bilayer, Biophys. J. 91 (2006) 3268–3275.
[41] R.G. Horn, Direct measurement of the force between two lipid bilayers and observation of their fusion, Biochim. Biophys. Acta 778 (1984) 224–228.
[42] I. Reviakine, A. Brisson, Formation of supported phospholipid bilayers from unilamellar vesicles investigated by atomic force microscopy, Langmuir 16 (2000) 1806–1815.
[43] K. El Kirat, I. Burton, V. Dupres, Y.F. Dufrene, Sample preparation procedures for biological atomic force microscopy, J. Microsc. 218 (2005) 199–207.
[44] M.C. Giocondi, S. Boichot, T. Plenat, C.C. Le Grimellec, Structural diversity of sphingomyelin microdomains, Ultramicroscopy 100 (2004) 135–143.
[45] S.J. Johnson, T.M. Bayerl, D.C. McDermott, G.W. Adam, A.R. Rennie, R.K. Thomas, E. Sackmann, Structure of an adsorbed dimyristoylphosphatidylcholine bilayer measured with specular reflection of neutrons, Biophys. J. 59 (1991) 289–294.
[46] E. Sackmann, Supported membranes: scientific and practical applications, Science 271 (1996) 43–48.

[47] Z. Shao, J. Mou, D.M. Czajkowsky, J. Yang, J.-Y. Yuan, Biological atomic force microscopy: what is achieved and what is needed, Adv. Phys. 1 (1996) 1–86.
[48] A. Sonnleitner, G.J. Schutz, T. Schmidt, Free brownian motion of individual lipid molecules in biomembranes, Biophys. J. 77 (1999) 2638–2642.
[49] D.A. Brown, J.K. Rose, Sorting of GPI-anchored proteins to glycolipid-enriched membrane subdomains during transport to the apical cell surface, Cell 68 (1992) 533–544.
[50] E. Mombelli, R. Morris, W. Taylor, F. Fraternali, Hydrogen-bonding propensities of sphingomyelin in solution and in a bilayer assembly: a molecular dynamics study, Biophys. J. 84 (2003) 1507–1517.
[51] R.E. Brown, Sphingolipid organization in biomembranes: what physical studies of model membranes reveal, J. Cell Sci. 111 (1998) 1–9.
[52] B. Ramstedt, J.P. Slotte, Membrane properties of sphingomyelins, FEBS Lett. 531 (2002) 33–37.
[53] B. Ramstedt, J.P. Slotte, Sphingolipids and the formation of sterol-enriched ordered membrane domains, Biochim. Biophys. Acta 1758 (2006) 1945–1956.